Multi-Beam Associated Coherent Integration Algorithm for Weak Target Detection

Xuan RAO [1,2], Zongying SUN [1], Haihong TAO [2]

[1] School of Information Engineering, Nanchang Hangkong University, Nanchang 330063, China
[2] National Laboratory of Radar Signal Processing, Xidian University, Xi'an 710071, China

raoxuancom@163.com

Submitted April 3, 2023 / Accepted October 2, 2023 / Online first December 9, 2023

Abstract. *Weak target detection is a great challenging in radar field. To detect the weak targets with beam migration, a novel tri-dimensional time model (i.e. fast time, slow time, and beam time) and a novel tri-dimensional signal model which based on the time model are set up firstly. Then, according to the presented models, we propose two multi-beam associated (MBA) coherent integration algorithms based on time-shared multi-beam (TSMB) and space-shared multi-beam (SSMB), respectively. The two proposed algorithms could both eliminate beam migration via associating multi-beam and realize coherent integration via discrete Fourier transform. According to different beam scanning modes, the subsequent analyses show that the MBA coherent integration algorithm based on SSMB (MBACIA-SSMB) may have a better detection performance than that based on TSMB (MBACIA-TSMB). Moreover, the capabilities to estimate the target's radial velocity and tangency velocity are analyzed. Finally, some numerical experiments are given to verify the performances of MBACIA-TSMB and MBACIA-SSMB.*

Keywords

Beam migration, coherent integration, multi-beam, weak target detection

1. Introduction

Weak moving target detection is widely studied in radar field. In general, the target with low radar cross section (RCS), high-speed and high-maneuvering target with limited available energy and the far-range target could be treated as weak targets [1], [2] These targets have a common characteristic, i.e., the signal-to-noise ratio (SNR) of target's echo is low and cannot be detected via traditional methods. An effective way to improve the detection performance of weak targets is increasing integration time. According to the echoes' phase information whether being utilized or not, the long time integration methods can be categorized into three kinds: coherent integration [3–18], incoherent integration[19–24] and hybrid integration. Compared with coherent integration, incoherent integration has a lower integration gain as the phase information is discarded. The integration gain of hybrid integration is better than that of incoherent integration but worse than that of coherent integration [25]. Thus, coherent integration has a best integration detection performance.

At present, the studies of weak target's coherent integration detection are focused on how to compensate range migration and Doppler migration effectively. To eliminate range migration, some typical methods are adopted, e.g., Keystone transform (KT) [8], [9], Hough transform (HT) [19–21], Radon transform (RT) [22], Dynamic programming (DP) [23], [24], second-order KT (SOKT) [26–29] and so on. Generally, the phase of echoes could be modeled as polynomial phase signal (PPS), so Fractional Fourier transform (FRFT) [5–7], Discrete Chirp-Fourier transform (DCFT) [17], [30] and so forth are adopted to compensate Doppler migration. In addition, some methods can compensate range migration and Doppler migration simultaneously, e.g. Generalized Radon-Fourier transform (GRFT) [14], [15], Radon-Fractional Fourier transform (RFRFT) [1], [16], Improved Axis Rotation Fractional Fourier transform (IAR-FRFT) [31] and Improved Axis Rotation Discrete Chip-Fourier transform (IAR-DCFT) [32], etc. Although the algorithms introduced above can compensate range/Doppler migration, the research of weak target's beam migration is scarce currently. On the one hand, with high-speed aircraft developing, the hypothesis that target lies in a beam during a coherent integrated time (CIT) maybe invalid. On the other hand, when the target echoes' energy, which is integrated in a beam, is not high enough, the coherent integration method based on multi-beam associated may be a potential way to detect the weaker target. So, it is necessary to study the detection of weak target with beam migration.

The remainder of this paper is organized as follows. In Sec. 2, we set up a tri-dimensional time model firstly, i.e., time divides into three parts: fast time, slow time, and beam time. Accordingly, a tri-dimensional signal model is proposed. Because radar multi-beam mode consists of time-shared multi-beam (TSMB) and space-shared multi-

DOI: 10.13164/re.2024.0001

beam (SSMB), we propose two multi-beam associated (MBA) coherent integration algorithms based on TSMB and SSMB respectively in Sec. 3. Subsequently, the algorithm flowcharts and performance analyses are given. In Sec. 4 some numerical experiments are provided to verify the performance of MBA coherent integration algorithm based on TSMB (MBACIA-TSMB) and MBA coherent integration algorithm based on SSMB (MBACIA-SSMB). Finally, some conclusions are given in Sec. 5.

2. Time Model and Signal Model

Suppose that the linear frequency modulated (LFM) pulse signal $p(t)$, which is transmitted by a phased array radar, may be written as

$$\begin{aligned} s_{\mathrm{t}}(t) &= p(t)\exp\left(\mathrm{j}2\pi f_{\mathrm{c}} t\right) \\ &= \mathrm{rect}\left(\frac{t}{T_{\mathrm{p}}}\right)\exp\left(\mathrm{j}\pi K_{\mathrm{r}} t^2\right)\exp\left(\mathrm{j}2\pi f_{\mathrm{c}} t\right) \end{aligned} \tag{1}$$

where $\mathrm{rect}\left(\frac{t}{T_{\mathrm{p}}}\right)=\begin{cases}1, & |t|\le T_{\mathrm{p}}/2\\ 0, & |t|>T_{\mathrm{p}}/2\end{cases}$, t is the time, T_{p} is the pulse duration, K_{r} is the chirp rate of LFM signal, and f_{c} is the radar carrier frequency.

$$\text{Let} \qquad t=\hat{t}+t_m+t_l=\hat{t}+mT_{\mathrm{pr}}+lT_{\mathrm{Bd}} \tag{2}$$

where $\hat{t}$ is the fast time, t_m is the slow time, m is the number of pulses, T_{pr} is the pulse repetition interval (PRI), and the pulse repetition frequency (PRF) equals $1/T_{\mathrm{pr}}$. t_l is defined as the beam time, l is the number of beams, T_{Bd} is the beam dwell time (BDT) which is the time that main beam dwell at some direction, the beam revisit frequency (BRF) equals $1/LT_{\mathrm{Bd}}$, and L is the total number of directions that beam should scan. Figure 1 shows the time model and the relationship between $\hat{t}$, t_m and t_l.

Suppose that the receiving array is a linear array, which consists of N antenna elements equally spaced a distance d apart. The elements are assumed to be isotropic radiators in that they have uniform response for signals from all directions [33]. When the beam points at direction θ_{d}, the sum of all outputs from the individual elements can be written as

$$\begin{aligned} Y_0 = A_{\mathrm{r}} &\frac{\sin\left(\frac{\pi Nd}{\lambda}\left(\sin\theta-\sin\theta_{\mathrm{d}}\right)\right)}{\sin\left(\frac{\pi d}{\lambda}\left(\sin\theta-\sin\theta_{\mathrm{d}}\right)\right)} \\ &\times\exp\left(\mathrm{j}\frac{\pi\left(N-1\right)d}{\lambda}\left(\sin\theta-\sin\theta_{\mathrm{d}}\right)\right) \end{aligned} \tag{3}$$

where A_{r} is the complex amplitude of the echo, λ is the wavelength and θ is the direction-of-arrival (DOA) of signal. The one-dimensional radiation pattern which points at direction θ_{d} may be

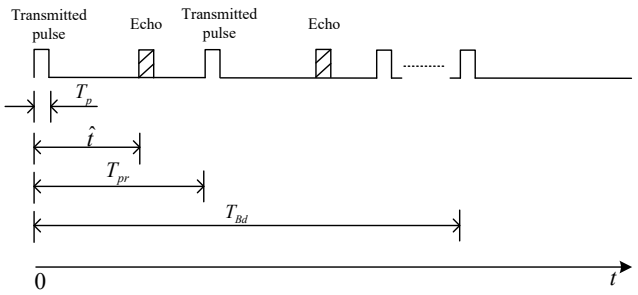

Fig. 1. Time model and relationship between $\hat{t}$, t_m and t_l ($t_m = mT_{\mathrm{pr}}$, $t_l = lT_{\mathrm{Bd}}$).

$$G(\theta)=\left|\frac{\sin\left(\frac{\pi Nd}{\lambda}\left(\sin\theta-\sin\theta_{\mathrm{d}}\right)\right)}{N\sin\left(\frac{\pi d}{\lambda}\left(\sin\theta-\sin\theta_{\mathrm{d}}\right)\right)}\right|. \tag{4}$$

Assume that the beam only scans along azimuth axis. Then, the beam scanning model of the radar is

$$\begin{aligned} &\theta_{\mathrm{d}}(t_l)=\theta_{\mathrm{d0}}+\left(\left(l\right)\right)_L\theta_{\mathrm{B,3dB}}, \\ &lT_{\mathrm{Bd}}\le t_l<\left(l+1\right)T_{\mathrm{Bd}},\ l=0,1,2,\ldots \end{aligned} \tag{5}$$

where θ_{d0} is the initial azimuth direction at which the beam points, $((\cdot))_L$ is the operation of modulo L and $\theta_{\mathrm{B,3\,dB}}$ is the half-power (3 dB) beamwidth.

Assume that there is a point scattering air target with a constant velocity v and the angle between radar boresight direction and the target motion direction is α. Thus, the target's radial motion model may be given as

$$R(t_m)=R_0+v_{\mathrm{r}}t_m,\quad m=0,1,2,\ldots,M,\ M=T_{\mathrm{Bd}}/T_{\mathrm{pr}} \tag{6}$$

where R_0 is the initial range, $v_{\mathrm{r}}=v\cos(\alpha)$ is the radial velocity. Accordingly, the target's tangency velocity v_{t} equals $v\sin(\alpha)$.

Consider that $R(t_m)$ is changing with t_m, the target's tangency motion model is nonlinear and may be provided as

$$\theta(t_m)=\theta_0+\theta_{\mathrm{v}}t_m,\ m=0,1,2,\ldots,M,\ M=T_{\mathrm{Bd}}/T_{\mathrm{pr}} \tag{7}$$

where θ_0 is the initial azimuth, θ_{v} is the angular velocity, θ_{a} is the angular acceleration. Accordingly, the target's tangency angular velocity $\theta_{\mathrm{v}}(t_m)=\theta_{\mathrm{v}}+\theta_{\mathrm{a}}t_m$. As we know, the relationship between angular velocity $\theta_{\mathrm{v}}(t_m)$ and tangency velocity v_{t} is

$$\theta_{\mathrm{v}}(t_m)=\frac{v_{\mathrm{t}}}{R(t_m)}. \tag{8}$$

Substituting (6) and $\theta_{\mathrm{v}}(t_m)=\theta_{\mathrm{v}}+\theta_{\mathrm{a}}t_m$ into (8) and neglecting the second-order term, we may get

$$\theta_{\mathrm{v}}=\frac{v_{\mathrm{t}}}{R_0} \tag{9}$$

and

$$\theta_{\mathrm{a}}=-\theta_{\mathrm{v}}\frac{v_{\mathrm{r}}}{R_0}. \tag{10}$$

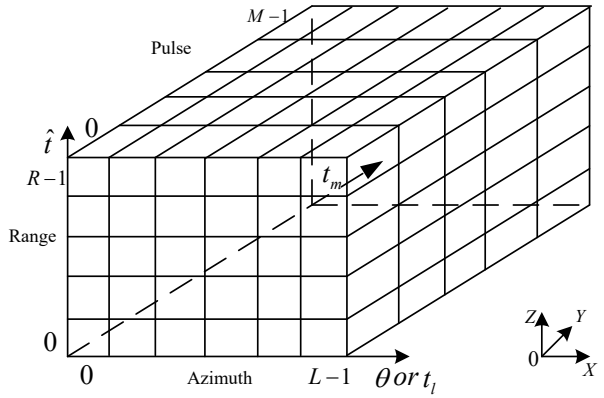

Fig. 2. Tri-dimensional signal model. X-axis represents the azimuth θ or beam time t_l; Y-axis represents the slow time t_m; Z-axis represents the fast time $\hat{t}$.

Assume that the radar works in far-field case and the initial range R_0 is several hundred kilometers, so θ_v is small while θ_a is nearly equal to zero which could be neglected. Thus, (7) could be simplified as

$$\theta(t_m) = \theta_0 + \theta_v t_m,\ m = 0,1,2,\ldots M,\ M = T_{Bd} / T_{pr}\ . \quad (11)$$

After coherent demodulation and pulse compression (PC), the tri-dimensional signal echo (Fig. 2) may be represented as

$$\begin{aligned} s(\hat{t},t_m,t_l) &= A\,\mathrm{sinc}\left(B\left(\hat{t}-\frac{2R(t_m)}{c}\right)\right)\exp\left(-\mathrm{j}\frac{4\pi}{\lambda}R(t_m)\right) \\ &\times\frac{\sin\left(\frac{N\pi d}{\lambda}\left(\sin(\theta(t_m))-\sin(\theta_d(t_l))\right)\right)}{\sin\left(\frac{\pi d}{\lambda}\left(\sin(\theta(t_m))-\sin(\theta_d(t_l))\right)\right)} \\ &\times\exp\left(\mathrm{j}\frac{N-1}{2}\frac{2\pi d}{\lambda}\left(\sin(\theta(t_m))-\sin(\theta_d(t_l))\right)\right) \end{aligned} \quad (12)$$

where A is the complex amplitude of echo after PC, $B = K_r \times T_p$ is the transmitted signal bandwidth and c is the speed of light.

Assume that the radar's beamwidth is relative narrow, the follow approximation may be established, i.e,

$$\sin(\theta(t_m)) \cong \theta(t_m), \quad (13)$$

$$\sin(\theta_d(t_l)) \cong \theta_d(t_l). \quad (14)$$

Let $d = \lambda/2$, and substituting (13) and (14) into (12), then

$$\begin{aligned} s(\hat{t},t_m,t_l) &= A\,\mathrm{sinc}\left(B\left(\hat{t}-\frac{2R(t_m)}{c}\right)\right)\exp\left(-\mathrm{j}\frac{4\pi}{\lambda}R(t_m)\right) \\ &\times\frac{\sin\left(\frac{N\pi}{2}\left(\theta(t_m)-\theta_d(t_l)\right)\right)}{\sin\left(\frac{\pi}{2}\left(\theta(t_m)-\theta_d(t_l)\right)\right)} \\ &\times\exp\left(\mathrm{j}\pi\frac{N-1}{2}\theta(t_m)\right)\exp\left(-\mathrm{j}\pi\frac{N-1}{2}\theta_d(t_l)\right). \end{aligned} \quad (15)$$

Substituting (6), (11) into (15), then

$$\begin{aligned} s(\hat{t},t_m,t_l) &= A\,\mathrm{sinc}\left(B\left(\hat{t}-\frac{2}{c}(R_0+v_r t_m)\right)\right) \\ &\times\exp\left(-\mathrm{j}\frac{4\pi}{\lambda}(R_0+v_r t_m)\right) \\ &\times\frac{\sin\left(\frac{N\pi}{2}\left((\theta_0-\theta_{d0})+\left(\theta_v t_m-\left((l)\right)_L\theta_{B,3dB}\right)\right)\right)}{\sin\left(\frac{\pi}{2}\left((\theta_0-\theta_{d0})+\left(\theta_v t_m-\left((l)\right)_L\theta_{B,3dB}\right)\right)\right)} \\ &\times\exp\left(\mathrm{j}\pi\frac{N-1}{2}(\theta_0+\theta_v t_m)\right) \\ &\times\exp\left(-\mathrm{j}\pi\frac{N-1}{2}\left(\theta_{d0}+\left((l)\right)_L\theta_{B,3dB}\right)\right). \end{aligned} \quad (16)$$

Let

$$\tilde{A} = A\frac{\sin\left(\frac{N\pi}{2}\left((\theta_0-\theta_{d0})+\left(\theta_v t_m-\left((l)\right)_L\theta_{B,3dB}\right)\right)\right)}{\sin\left(\frac{\pi}{2}\left((\theta_0-\theta_{d0})+\left(\theta_v t_m-\left((l)\right)_L\theta_{B,3dB}\right)\right)\right)}\exp\left(-\mathrm{j}\frac{4\pi}{\lambda}R_0\right)$$

$\times\exp\left(\mathrm{j}\pi\frac{N-1}{2}\theta_0\right)$, then (16) can be rewritten as

$$\begin{aligned} s(\hat{t},t_m,t_l) &= \tilde{A}\,\mathrm{sinc}\left(B\left(\hat{t}-\frac{2}{c}(R_0+v_r t_m)\right)\right) \\ &\times\exp\left(-\mathrm{j}\frac{4\pi}{\lambda}v_r t_m\right)\exp\left(\mathrm{j}\pi\frac{N-1}{2}\theta_v t_m\right) \\ &\times\exp\left(-\mathrm{j}\pi\frac{N-1}{2}\left(\theta_{d0}+\left((l)\right)_L\theta_{B,3dB}\right)\right). \end{aligned} \quad (17)$$

Define T_{across} as the time that the target flies across $\theta_{B,3\,dB}$, then

$$v_t T_{across} = R_0\theta_{B,3dB} \quad (18)$$

where

$$\theta_{B,3dB} = \frac{\lambda}{D} = \frac{\lambda}{(N-1)d} = \frac{2}{N-1} \quad (19)$$

and D is antenna dimension.

According to (9), (18), (19), we can obtain

$$\theta_v = \frac{v_t}{R_0} = \frac{2/(N-1)}{T_{across}}\ . \quad (20)$$

Substituting (20) into (16), the tri-dimensional echo signal may be given as

$$\begin{aligned} s(\hat{t},t_m,t_l) &= \tilde{A}\,\mathrm{sinc}\left(B\left(\hat{t}-\frac{2}{c}(R_0+v_r t_m)\right)\right) \\ &\times\exp\left(-\mathrm{j}\frac{4\pi}{\lambda}v_r t_m\right)\exp\left(\mathrm{j}\pi\frac{1}{T_{across}}t_m\right) \\ &\times\exp\left(-\mathrm{j}\pi\frac{N-1}{2}\left(\theta_{d0}+\left((l)\right)_L\theta_{B,3dB}\right)\right). \end{aligned} \quad (21)$$

The target's Doppler frequency is defined as

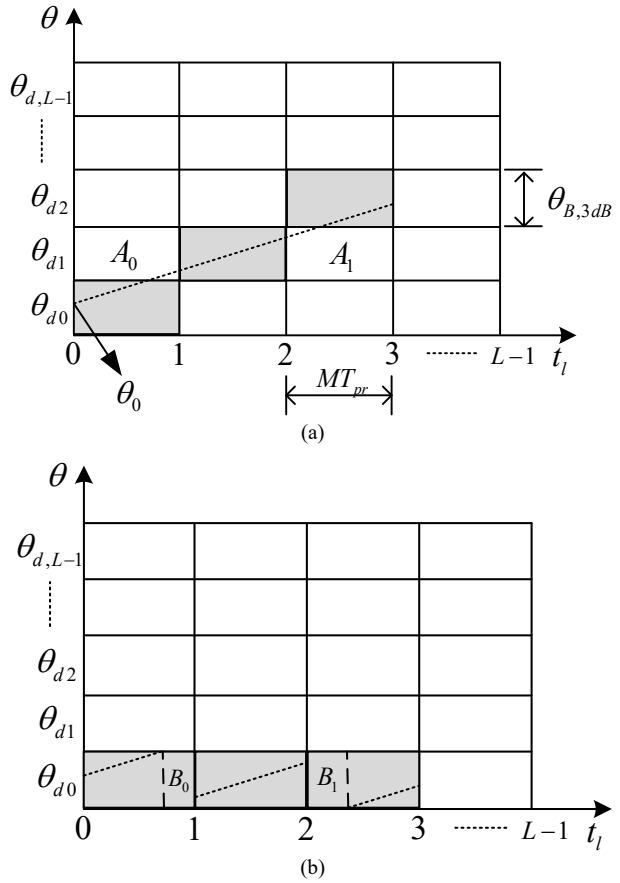

Fig. 3. Process of MBACIA-TSMB. (a) The relationship between target's azimuth and the azimuth direction at which the beam points. And target's azimuth and the beam direction are superposed at the shadow regions. (b) The echoes in different beams are concentrated in a beam via multi-beam association process.

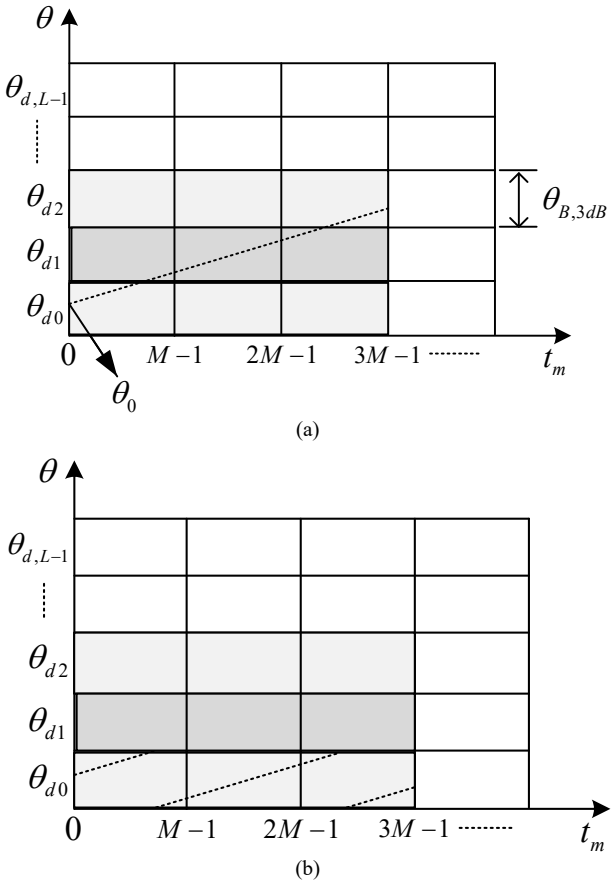

Fig. 4. Process of MBACIA-SSMB. (a) The relationship between target's azimuth and the azimuth direction at which the beam points. Different shadow regions represent different beams. (b) The echoes in different beams are concentrated in a beam via multi-beam association process.

$$f_{\mathrm{d,r}} = 2v_{\mathrm{r}} / \lambda \,. \tag{22}$$

Moreover, to estimate the target's tangency velocity, we extend the concept of Doppler frequency to tangency Doppler frequency, which is defined as

$$f_{\mathrm{d,t}} = 1/\left(2T_{\mathrm{across}}\right). \tag{23}$$

We define $f_{\mathrm{d,r}}$ as a positive frequency when the target moves toward the radar, and $f_{\mathrm{d,t}}$ is a positive frequency when the target flies across $\theta_{\mathrm{B,3\,dB}}$ in a clockwise direction (i.e., from left to right). Then (21) may be represented as

$$\begin{aligned} s\left(\hat{t}, t_m, t_l\right) = \tilde{A}\,\mathrm{sinc}&\left(B\left(\hat{t} - \frac{2}{c}\left(R_0 + v_{\mathrm{r}} t_m\right)\right)\right) \\ &\times \exp\left(-\mathrm{j}2\pi f_{\mathrm{d,r}} t_m\right)\exp\left(\mathrm{j}2\pi f_{\mathrm{d,t}} t_m\right) \\ &\times \exp\left(-\mathrm{j}\pi \frac{N-1}{2}\left(\theta_{\mathrm{d0}} + \left(\left(l\right)\right)_L \theta_{\mathrm{B,3dB}}\right)\right). \end{aligned} \tag{24}$$

In (24), the first exponential term is the phase value caused by target's radial motion. The second exponential term is the phase value caused by target's tangency motion. The third exponential term is the phase value caused by the azimuth direction at which the beam points.

3. Coherent Integration Algorithm for Weak Target with Beam Migration

According to the different radar systems, multi-beam mode consists of TSMB and SSMB. In this section, we propose two MBA coherent integration algorithms based on TSMB and SSMB respectively, i.e. MBACIA-TSMB and MBACIA-SSMB. Subsequently, the algorithm flowcharts and performance analyses are given.

3.1 MBACIA-TSMB

That the multi-beam is generated in a time sequential (time-shared) manner is regarded as TSMB. Figure 3(a) shows the relationship between the azimuth direction at which the beam points and target's azimuth.

In Fig. 3(a), θ represents azimuth. θ_{d0}, θ_{d1}, θ_{d2},…,$\theta_{\mathrm{d},L-1}$ are the L directions that beam should scan. t_l is the beam time. The beam point at θ_{d0} when $l = 0$, the beam point at $\theta_{\mathrm{d1}} = \theta_{\mathrm{d0}} + \theta_{\mathrm{B,3\,dB}}$ when $l = 1$, and so on. The shadow regions represent the different beam directions in different beam time. The broken line is the motion track of a moving

target. The initial azimuth of the target is θ_0, and the target flies across several beams during the observation time. It should be noticed that the target's azimuth and the beam direction are superposed at the shadow regions. So, there are no target's echoes when the target lies in the region A_0 and A_1.

To detect the weak target with beam migration, coherent integration is an effective method. Although the received signal is continuous in time, the signal's phases are different in different azimuths, i.e., the third exponential term in (24) is different for different beam directions. So, we can realize multi-beam associated coherent integration via compensating the third exponential term, i.e., MBACIA-TSMB. Let us define a phase compensation factor

$$F_{((l))_L}^{\text{phase}} = \exp\left(\text{j}\pi \frac{N-1}{2} \left((l) \right)_L \theta_{\text{B,3dB}} \right). \tag{25}$$

Then, the received signal may be rewritten as

$$s'\left(\hat{t}, t_m, t_l\right) = \begin{cases} s\left(\hat{t}, t_m, t_l\right) \times F_0^{\text{phase}}, 0 \le t_l < T_{\text{Bd}} \\ s\left(\hat{t}, t_m, t_l\right) \times F_1^{\text{phase}}, \ T_{\text{Bd}} \le t_l < 2T_{\text{Bd}} \\ \cdots \quad , \quad \cdots \end{cases}. \tag{26}$$

Figure 3(b) shows that the signal received from different beam directions may be regarded as a signal received from a same beam direction by adopting the phase compensation factor. It is also known that the beam migration has been eliminated. Subsequently, the coherent integration algorithm for weak target without beam migration may be performed, e.g., Moving Target Detection (MTD) [33], Improved Axis Rotation MTD (IAR-MTD) [34], and so on. However, it should be noticed that there are no target's echoes in the region B_0 and B_1.

3.2 MBACIA-SSMB

That the multi-beam is generated in a space-shared manner is regarded as SSMB, i.e., radar forms several beams at the same time. That means several beams point at θ_{d0}, θ_{d1}, θ_{d2},…,$\theta_{\text{d},L-1}$ simultaneously whether what l equals. So, (2) may be degraded into

$$t = \hat{t} + t_m = \hat{t} + mT_{\text{pr}} \tag{27}$$

where m = 0,1,2,…. And (5) may be transformed into

$$\theta_{\text{d}l} = \theta_{\text{d0}} + l\theta_{\text{B,3dB}}, l = 0,1,2,\ldots L-1. \tag{28}$$

Then, (12) may be represented as

$$\begin{aligned} s\left(\hat{t}, t_m, \theta_{\text{d}l}\right) = A \,\text{sinc}\left(B\left(\hat{t} - \frac{2R\left(t_m\right)}{c} \right) \right) \exp\left(-\text{j}\frac{4\pi}{\lambda} R\left(t_m\right) \right) \\ \times \frac{\sin\left(\frac{N\pi d}{\lambda} \left(\sin\left(\theta\left(t_m\right)\right) - \sin\left(\theta_{\text{d}l}\right) \right) \right)}{\sin\left(\frac{\pi d}{\lambda} \left(\sin\left(\theta\left(t_m\right)\right) - \sin\left(\theta_{\text{d}l}\right) \right) \right)} \\ \times \exp\left(\text{j}\frac{N-1}{2} \frac{2\pi d}{\lambda} \left(\sin\left(\theta\left(t_m\right)\right) - \sin\left(\theta_{\text{d}l}\right) \right) \right), \\ l = 0,1,2,\ldots L-1. \end{aligned} \tag{29}$$

Similarly, (24) may be rewritten as

$$\begin{aligned} s\left(\hat{t}, t_m, \theta_{\text{d}l}\right) = \tilde{A} \,\text{sinc}\left(B\left(\hat{t} - \frac{2}{c}\left(R_0 + v_{\text{r}} t_m \right) \right) \right) \\ \times \exp\left(-\text{j}2\pi f_{\text{d,r}} t_m \right) \exp\left(\text{j}2\pi f_{\text{d,t}} t_m \right) \\ \times \exp\left(-\text{j}\pi \frac{N-1}{2} \left(\theta_{\text{d0}} + l\theta_{\text{B,3dB}} \right) \right), l = 0,1,2,\ldots L-1 \end{aligned} \tag{30}$$

where

$$\begin{aligned} \tilde{A} = A \frac{\sin\left(\frac{N\pi}{2} \left(\left(\theta_0 - \theta_{\text{d0}} \right) + \left(\theta_{\text{v}} t_m - l\theta_{\text{B,3dB}} \right) \right) \right)}{\sin\left(\frac{\pi}{2} \left(\left(\theta_0 - \theta_{\text{d0}} \right) + \left(\theta_{\text{v}} t_m - l\theta_{\text{B,3dB}} \right) \right) \right)} \exp\left(-\text{j}\frac{4\pi}{\lambda} R_0 \right) \\ \times \exp\left(\text{j}\pi \frac{N-1}{2} \theta_0 \right). \end{aligned}$$

Figure 4(a) gives the relationship between the azimuth direction at which the beam points and target's azimuth. t_m represents the slow time. θ represents azimuth. θ_{d0}, θ_{d1}, θ_{d2},…,$\theta_{\text{d},L-1}$ are the L directions that beam should cover. Similar to Fig. 3, there is a same moving target and the broken line represents the target's motion track. Because L directions are covered by beam simultaneously, the received signal of radar includes target's all echoes, which is different from the case in TSMB.

To detect weak target with beam migration in SSMB mode, a coherent integration algorithm MBACIA-SSMB is proposed as follows. Firstly, a phase compensation factor is defined as

$$F_l^{\text{phase}} = \exp\left(\text{j}\pi \frac{N-1}{2} l\theta_{\text{B,3dB}} \right), l = 0,1,2,\ldots L-1. \tag{31}$$

Then, the received signal of different beams may be written as

$$s'\left(\hat{t}, t_m, \theta_{\text{d}l}\right) = \begin{cases} s\left(\hat{t}, t_m, \theta_{\text{d}l}\right) \times F_0^{\text{phase}}, l = 0 \\ s\left(\hat{t}, t_m, \theta_{\text{d}l}\right) \times F_1^{\text{phase}}, l = 1 \\ \cdots \quad , \quad \cdots \\ s\left(\hat{t}, t_m, \theta_{\text{d}l}\right) \times F_{L-1}^{\text{phase}}, l = L-1 \end{cases} \tag{32}$$

Finally, these signals are summed together, then we obtain

$$s''\left(\hat{t}, t_m\right) = \sum_{l=0}^{L-1} s'\left(\hat{t}, t_m, \theta_{\text{d}l}\right) \times F_l^{\text{phase}}. \tag{33}$$

Figure 4(b) shows that the signal received from different beam directions may be regarded as a signal received from a same beam direction via phase compensation and the operation of sum. Because the beam migration has been compensated, the coherent integration algorithm for weak target without beam migration may be adopted subsequently, e.g., MTD, IAR-MTD, and so on.

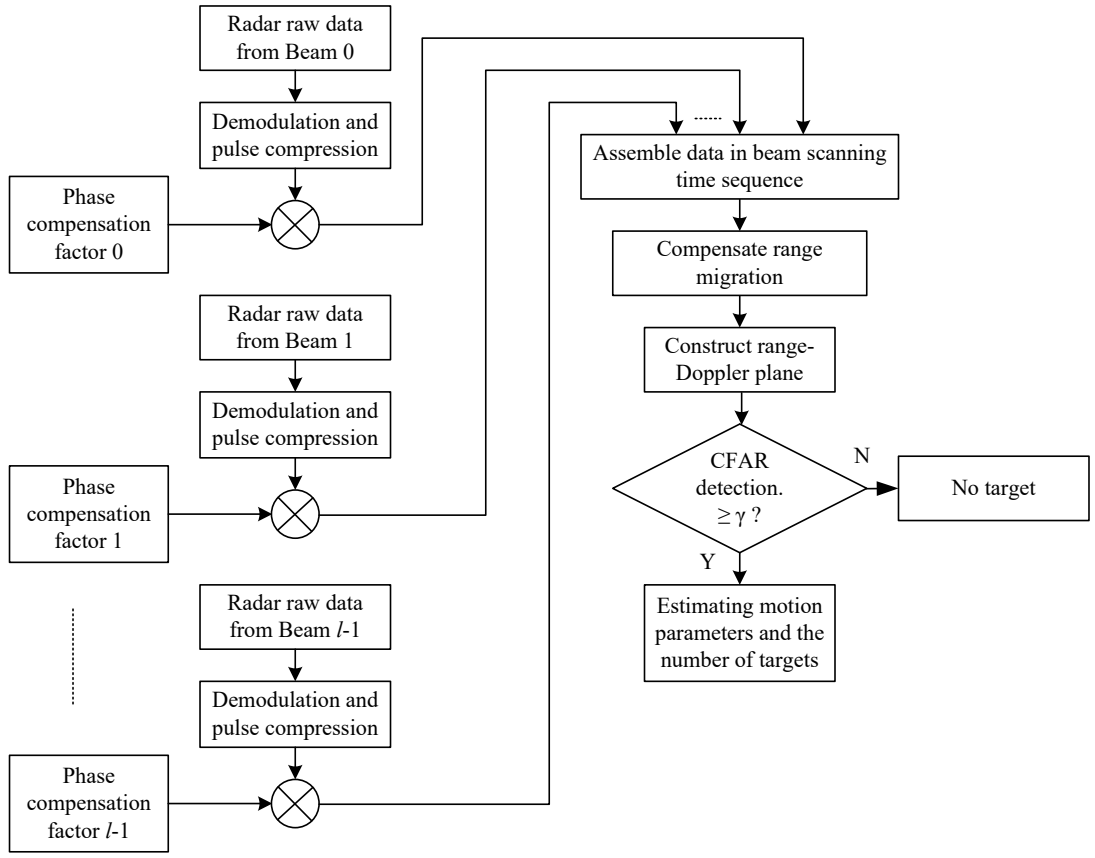

(a)

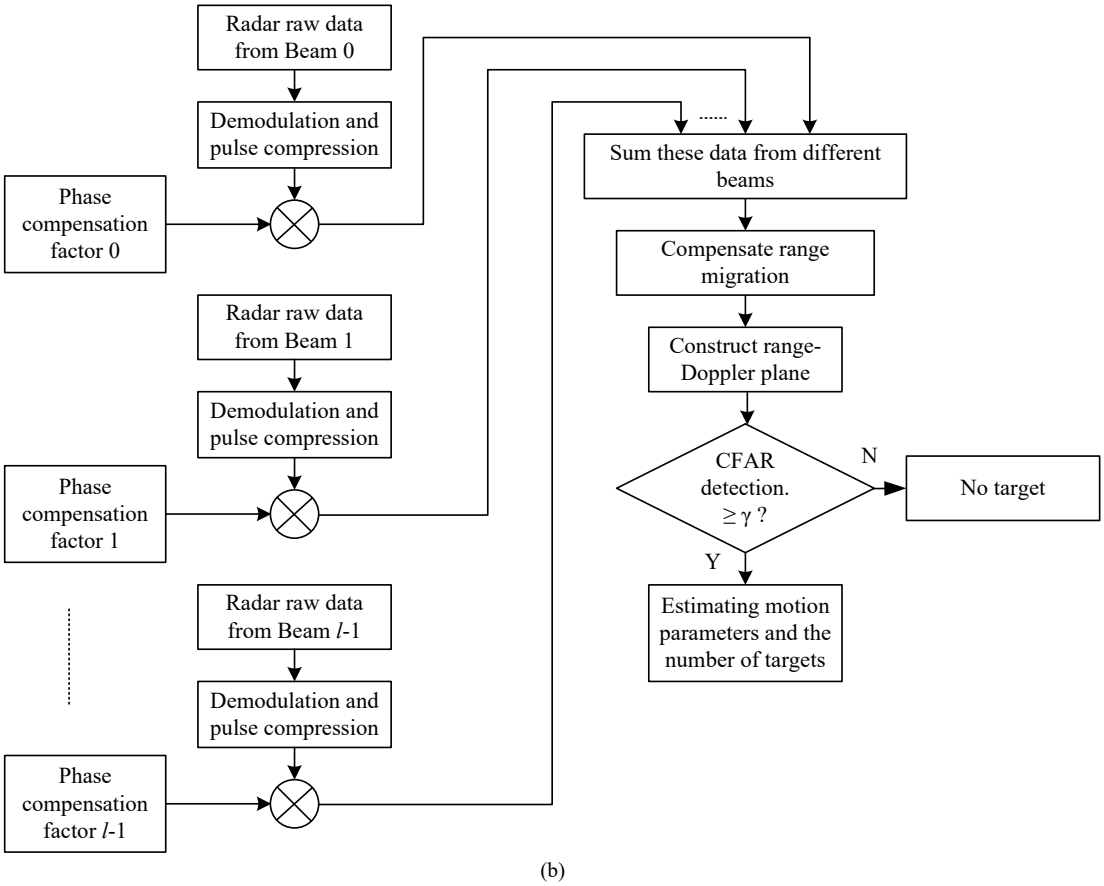

(b)

Fig. 5. Flowcharts of multi-beam associated coherent integration algorithm. (a) Flowchart of MBACIA-TSMB. (b) Flowchart of MBACIA-SSMB.

3.3 Algorithm Flowchart and Performance Analysis

3.3.1 Algorithm Flowchart

Figure 5 gives the flowcharts of MBACIA-TSMB and MBACIA-SSMB, respectively. In Fig. 5(a), the number of beams should be associated, i.e., l, is predetermined firstly according to radar parameters, dwell time of antenna beam T_{Bd}, half-power beamwidth $\theta_{\mathrm{B,3\ dB}}$ and the prior knowledge of target's tangency velocity. Then, demodulation, PC and phase compensation are completed, respectively. Subsequently, the different data from the different beams will be assembled in beam scanning time sequence. Thus the beam migration is eliminated and all data have been concentrated in a beam. Then, to compensate range migration and realize coherent integration, the coherent integration algorithm for weak target without beam migration (e.g., IAR-MTD) may be adopted subsequently. Furthermore, the range-Doppler plane is constructed via Fast Fourier transform (FFT). Finally, carry out the constant false alarm ratio (CFAR) detection to confirm a target. If targets exist, the motion parameters and the number of the targets will be estimated. Except that l is determined by radar work mode and the data from different beams will be summed up, the other processes in Fig. 5(b) are identical to those in Fig. 5(a).

3.3.2 Performance Analysis

MBACIA-TSMB can increase CIT via compensating phase difference of different beams. However, because both the radar's beam and the target are moving, the number of collected target's echoes may decrease, which will result in the coherent integration gain decreasing. MBACIA-SSMB can also increase CIT and may collect target's all echoes because radar's beams cover all directions of interest. However, the summation of all data of different beams will lead to noise power increasing. So, the choice of l will affect the coherent integration performance.

As we know, Discrete Fourier transform (DFT) can serve as Doppler filter banks to detect a moving target. For the weak target with constant velocity, carry out FFT along slow time dimension will result in a peak in some frequency. So it seems that the peak may appear at $(-f_{\mathrm{d,r}}+f_{\mathrm{d,t}})$ according to (26) or (30) and $f_{\mathrm{d,r}}$, $f_{\mathrm{d,t}}$ cannot be distinguished.

But, in fact, $f_{\mathrm{d,r}}$ and $f_{\mathrm{d,t}}$ can be distinguished. On the one hand, according to (22) and (23), we can know that $|f_{\mathrm{d,r}}| >> |f_{\mathrm{d,t}}|$ in general when $v_{\mathrm{r}} \neq 0$. On the other hand, it is well known that the Doppler frequency resolution is decided by the effective observation time, i.e., CIT. Therefore, $f_{\mathrm{d,r}}$ may be estimated firstly by Doppler filter banks with low Doppler frequency resolution via a shorter CIT. And then compensate the phase of echoes via $\exp(\mathrm{j}2\pi f_{\mathrm{d,r}} t_m)$. Finally, $f_{\mathrm{d,t}}$ may be estimated by Doppler filter banks with high Doppler frequency resolution via a longer CIT.

4. Simulations and Comparisons

To verify the performance of MBACIA-TSMB and MBACIA-SSMB, some numerical experiments are provided in this section. The experiment parameters are given as follows: $N = 178$, $\theta_{\mathrm{d0}} = 0$ rad, $\theta_{\mathrm{B,3\ dB}} = 0.01$ rad, $\theta_0 = 0.003$ rad, $R_0 = 100$ km, $f_{\mathrm{c}} = 150$ MHz, $B = 10$ MHz, $T_{\mathrm{p}} = 5$ μs, $G_{\mathrm{PC}} = 10\log_{10}(T_{\mathrm{p}} \times B) = 16.99$ dB, $PRF = 30$ kHz, $f_{\mathrm{s}} = B$, CIT $T_{\mathrm{integration}} = 1$ s, false alarm probability $P_{\mathrm{fa}} = 10^{-6}$, the number of Monte Carlo experiments is 200 times.

4.1 Simulation 1

The first simulation example shows the performance of MBACIA-TSMB. The motion parameters of a moving target are given as follows: $v_{\mathrm{t}} = 10$ km/s ≅ 30 Mach ($\theta_{\mathrm{v}} = 0.1$ rad/s), $v_{\mathrm{r}} = 0$ m/s. The beam scanning parameters are: $T_{\mathrm{Bd}} = 0.1$ s, $L = 10$. The input SNR is assumed to be 0 dB.

Figure 6(a) shows that the target's echoes are distributed in the first three beams. The echoes are not continuous for the asynchronism in azimuth direction between beam and target. After the initial observe time, there are no target's echoes in the radar's received signal. The target's echoes are concentrated in a beam via MBA based on TSMB. Then, Figure 6(b) shows the range-slow time plane in a beam. Because of $v_{\mathrm{r}} = 0$, there is no range migration. Carry out FFT, and then the peak in Fig. 6(c) represents the target's tangency Doppler frequency, i.e., $f_{\mathrm{d,t}} = 5$ Hz, $v_{\mathrm{t}} = 10$ km/s.

4.2 Simulation 2

The performance of MBACIA-SSMB is presented in the second simulation example. Because the beam points at $L = 10$ directions simultaneously, beam dwell time does not exist in this simulation. The other parameters are identical to those in the first simulation.

Although it is similar to the first simulation that the target's echoes are distributed in ten beams, the echoes are continuous for ten beams covering ten azimuth directions at the same time (Fig. 7(a)). After the process of MBA based on SSMB, the target's echoes are concentrated in a beam. Similarly, there is also no range migration for $v_{\mathrm{r}} = 0$ (Fig. 7(b)). The peak in Fig. 7(c) represents the target's tangency Doppler frequency. However, it should be noticed that the peak value in Fig. 7(c) is greater than that in Fig. 6(c) because more target's echoes are integrated.

4.3 Simulation 3

The detection performances of MBACIA-TSMB and MBACIA-SSMB are compared in the third simulation example. We assume that the input SNR varies from −40 to −15 dB, the relationship curve between the detection prob-

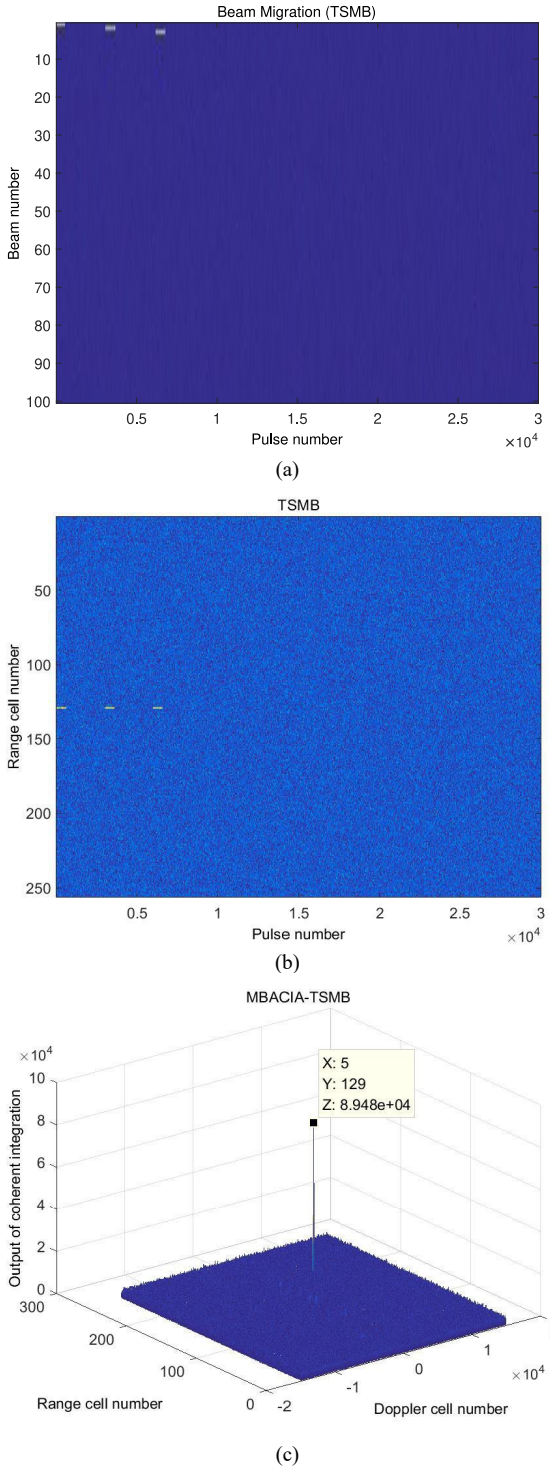

Fig. 6. Detection of weak target via MBACIA-TSMB. (a) Target's echoes are distributed in the first three beams; (b) After compensate beam migration, the target's echoes lie in the range-slow time plane of a beam; (c) Output of coherent integration (v_t = 10 km/s, $f_{d,t}$ = 5 Hz).

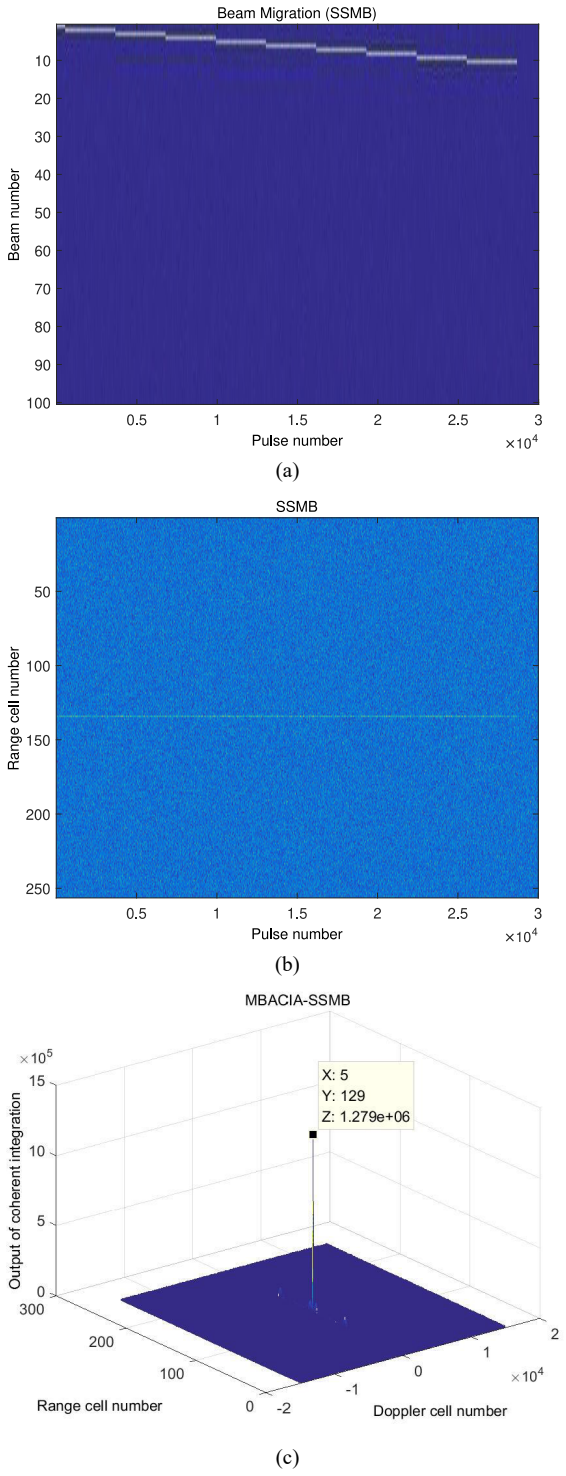

Fig. 7. Detection of weak target via MBACIA-SSMB. (a) Target's echoes are distributed in all ten beams; (b) After compensate beam migration, the target's echoes lie in the range-slow time plane of a beam; (c) Output of coherent integration (v_t = 10 km/s, $f_{d,t}$ = 5 Hz).

ability (Pd) and the input SNR is shown in Fig. 8. It is clear that the detection performance of MBACIA-SSMB is better than that of MBACIA-TSMB for more target's echoes being integrated. However, the benefit of detection performance results from system complexity increasing. So, in some applications, a hybrid scheme based on the two algorithms may be a good compromise between system complexity and detection performance.

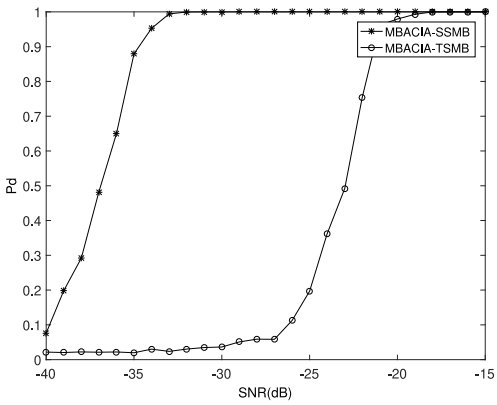

Fig. 8. Detection performance comparison between MBACIA -TSMB and MBACIA-SSMB.

4.4 Simulation 4

According to the analysis in Sec. 3.3.2, we know that MBACIA-TSMB and MBACIA-SSMB have the capability of estimating target's radial velocity and tangency velocity. The performance is verified in the fourth simulation example via MBACIA-SSMB. The input SNR is assumed to be −10 dB. The part motion parameters of a moving target are given as follows: $v_t = 10$ km/s ≅ 30 Mach ($\theta_v = 0.1$ rad/s), $v_r = -100$ m/s. It should be noticed that $v_r = -100$ m/s is only for simplicity, i.e., there is no range migration during CIT. If range migration happens, it should be eliminated firstly before coherent integration. Figure 9(a) shows that Doppler frequency is estimated via a shorter integration time (0.01 s). And then, compensate the phase of echoes via the estimated Doppler frequency, i.e., $\exp(j2\pi f_{d,r} t_m)$. Finally, tangency Doppler frequency may be detected via a longer integration time (1 s) (Fig. 9(b)). It is clear that the precision of Doppler frequency is better than that of tangency Doppler frequency. If the phase of echoes does not be compensated, the output peak will appear on the frequency, which equals the sum of Doppler frequency and tangency Doppler frequency (Fig. 9(c)). To compare conveniently, we let $v_t = 0$ m/s. Then, Figure 9(d) shows that the Doppler frequency $f_{d,r} = -100$ Hz, which is estimated via a longer integration time (1 s).

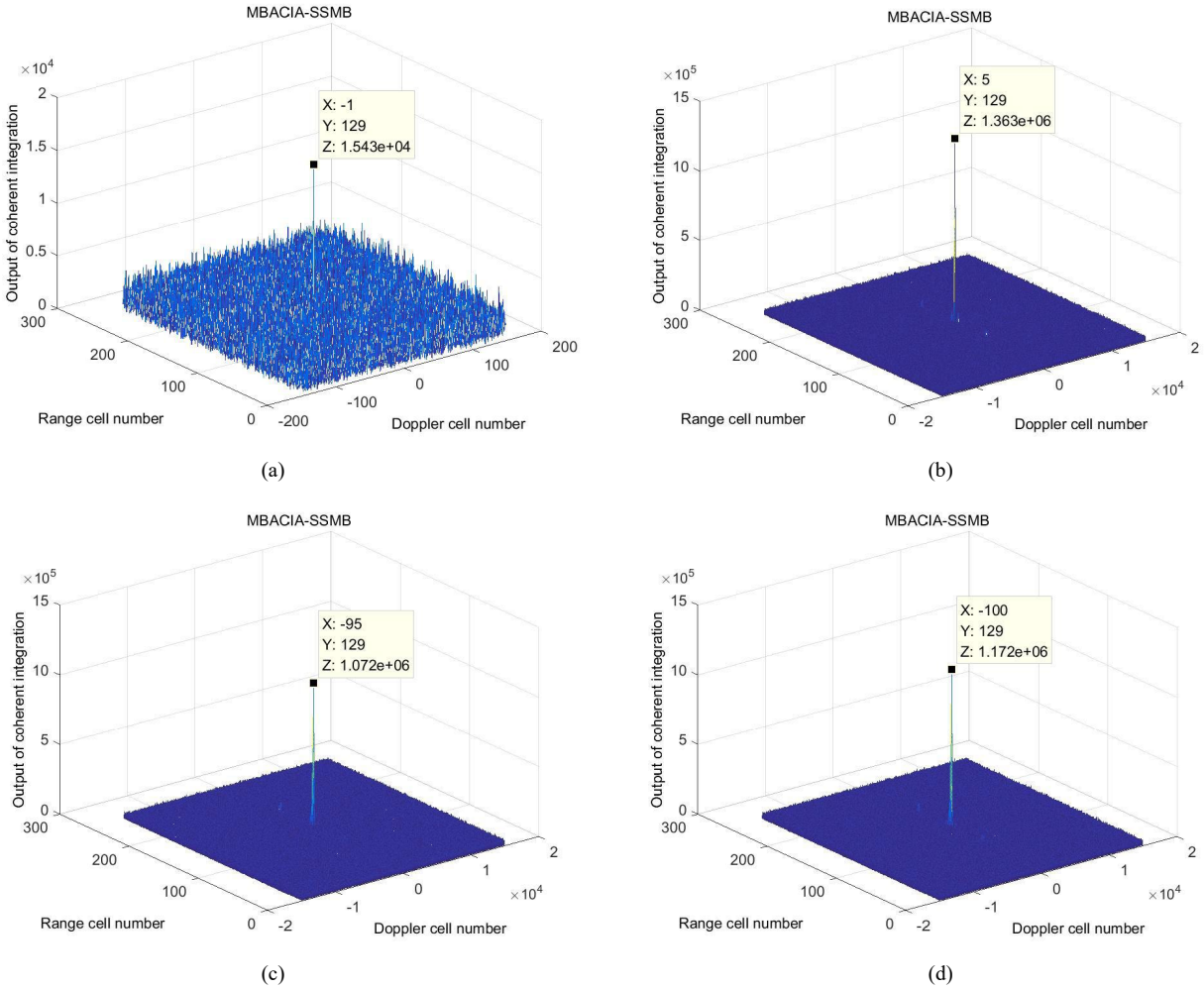

Fig. 9. Estimation of target's Doppler frequency and tangency Doppler frequency. (a) Target's Doppler frequency is estimated via a shorter CIT (0.01 s), ($v_r = -100$ m/s, $f_{d,r} = -1$ Hz); (b) Target's tangency Doppler frequency is estimated via a longer CIT (1 s) after Doppler frequency compensation, ($v_t = 10$ km/s, $f_{d,t} = 5$ Hz); (c) If Doppler frequency is not compensated, the estimated frequency will be the sum of Doppler frequency and tangency Doppler frequency, ($v_r = -100$ m/s, $v_t = 10$ km/s, $f_{d,t} + f_{d,t} = -95$ Hz); (d) Target's Doppler frequency is estimated via a longer CIT (1 s) when $v_r = 0$ m/s, ($v_r = -100$ m/s, $v_t = 0$ m/s, $f_{d,t} = -100$ Hz).

5. Conclusion

To detect weak target with beam migration, we set up a novel tri-dimensional time model and a novel tri-dimensional signal model. According to different beam scanning modes, two MBA coherent integration algorithms, i.e., MBACIA-TSMB and MBACIA-SSMB, are proposed respectively. Then, the subsequent analysis shows that the MBACIA-SSMB may have a better detection performance than MBACIA-TSMB. But, what is sacrificed is the increasing of system complexity. So, in some applications, a hybrid scheme based on the two algorithms may be a good compromise between system complexity and detection performance. Moreover, the capability of estimating target's radial velocity and tangency velocity is analyzed. Although the precision of tangency Doppler frequency is lower than that of Doppler frequency, a potential way of estimating tangency velocity via long coherent integration is presented. The future work along this direction is increasing the estimation precision of tangency velocity by combining target track technique.

Acknowledgments

The authors would like to thank the anonymous reviewers and the Associate Editor. This work is supported by the National Nature Science Foundation of China under Grant 62161029, Jiangxi Provincial Natural Science Foundation under Grants 20202BABL202002, SAST2018078, the Doctoral Scientific Research Foundation of NCHU under Grant EA201804195.

References

[1] CHEN, X. L., GUAN, J., LIU, N., et al. Maneuvering target detection via Radon-fractional Fourier transform-based long-time coherent integration. *IEEE Transactions on Signal Processing*, 2014, vol. 62, no. 4, p. 939–953. DOI: 10.1109/TSP.2013.2297682

[2] WEI, S., DAI, Y., ZHANG, Q. Weak and maneuvering target detection with long observation time based on segment fusion for narrowband radar. *Sensors*, 2022, vol. 22, no. 18, p. 1–24. DOI: 10.3390/s22187086

[3] ZHANG, Z., LIU, N., HOU, Y., et al. A coherent integration segment searching based GRT-GRFT hybrid integration method for arbitrary fluctuating target. *Remote Sensing*, 2022, vol. 14, no. 11, p. 1–20. DOI: 10.3390/rs14112695

[4] CAO, Y.-F., WANG, W.-Q., ZHANG, S. Long-time coherent integration for high-order maneuvering target detection via zero-trap line extraction. *IEEE Transactions on Aerospace and Electronic Systems*, 2021, vol. 57, no. 6, p. 4017–4027. DOI: 10.1109/TAES.2021.3082718

[5] TAO, R., LI, Y. L., WANG, Y. Short-time fractional Fourier transform and its applications. *IEEE Transactions on Signal Processing*, 2009, vol. 58, no. 5, p. 2568–2580. DOI: 10.1109/TSP.2009.2028095

[6] QI, L., TAO, R., ZHOU, S., et al. Detection and parameter estimation of multicomponent LFM signal based on the fractional Fourier transform. *Science in China Series F: Information Science*, 2004, vol. 47, no. 2, p. 184–198. DOI: 10.1360/02yf0456

[7] GUAN, J., CHEN, X. L., HUANG Y., et al. Adaptive fractional Fourier transform-based detection algorithm for moving target in heavy sea clutter. *IET Radar, Sonar & Navigation*, 2012, vol. 6, no. 5, p. 389–401. DOI: 10.1049/iet-rsn.2011.0030

[8] DAI, Z., ZHANG, X., FANG, H., et at. High accuracy velocity measurement based on keystone transform using entropy minimization. *Chinese Journal of Electronics*, 2016, vol. 25, no. 4, p. 774–778. DOI: 10.1049/cje.2016.06.009

[9] ZHANG, S., ZENG, T., LONG, T., et al. Dim target detection based on keystone transform. In *IEEE International Radar Conference.* Arlington (VA, USA), 2005, p. 889–894 DOI: 10.1109/RADAR.2005.1435953

[10] SU, J., XING, M., WANG, G., et al. High-speed multi-target detection with narrowband radar. *IET Radar, Sonar & Navigation*, 2010, vol. 4, no. 4, p. 595–603. DOI: 10.1049/iet-rsn.2008.0160

[11] XU, J., YU, J., PENG, Y. N., et al. Radon-Fourier transform for radar target detection, I: Generalized Doppler filter bank. *IEEE Transactions on Aerospace and Electronic Systems*, 2011, vol. 47, no. 2, p. 1186–1202. DOI: 10.1109/TAES.2011.5751251

[12] XU, J., YU, J., PENG, Y. N., et al. Radon-Fourier transform for radar target detection (II): Blind speed sidelobe suppression. *IEEE Transactions on Aerospace and Electronic Systems*, 2011, vol. 47, no. 4, p. 2473-2489. DOI: 10.1109/TAES.2011.6034645

[13] YU, J., XU, J., PENG, Y. N., et al. Radon-Fourier transform for radar target detection (III): Optimality and fast implementations. *IEEE Transactions on Aerospace and Electronic Systems*, 2012, vol. 48, no. 2, p. 991–1004. DOI: 10.1109/TAES.2012.6178044

[14] XU, J., XIA, X. G., PENG, S. B., et al. Radar maneuvering target motion estimation based on generalized Radon-Fourier transform. *IEEE Transactions on Signal Processing*, 2012, vol. 60, no. 12, p. 6190–6201. DOI: 10.1109/TSP.2012.2217137

[15] MA, B., ZHANG, S., JIA, W., et at. Fast implementation of generalized Radon–Fourier transform. *IEEE Transactions on Aerospace and Electronic Systems*, 2021, vol. 57, no. 6, p. 3758 to 3767. DOI: 10.1109/TAES.2021.3082717

[16] GAO, C., TAO, R., KANG, X. Weak target detection in the presence of sea clutter using Radon-Fractional Fourier transform canceller. *IEEE Journal of Selected Topics in Applied Earth Observations and Remote Sensing*, 2021, vol. 14, p. 5818–5830. DOI: 10.1109/JSTARS.2021.3078723

[17] XIA, X. G. Discrete chirp-Fourier transform and its application to chirp rate estimation. *IEEE Transactions on Signal Processing*, 2000, vol. 48, no. 11, p. 3122–3133. DOI: 10.1109/78.875469

[18] WU, L., WEI, X., YANG, D., et al. ISAR imaging of targets with complex motion based on discrete chirp Fourier transform for cubic chirps. *IEEE Transactions on Geoscience and Remote Sensing*, 2012, vol. 50, no. 10, p. 4201–4212. DOI: 10.1109/TGRS.2012.2189220

[19] CARLSON, B. D., EVANS, E. D., WILSON, S. L. Search radar detection and track with the Hough transform. I. System concept. *IEEE Transactions on Aerospace and Electronic Systems*, 1994, vol. 30, no. 1, p. 102–108. DOI: 10.1109/7.250410

[20] CARLSON, B. D., EVANS, E. D., WILSON, S. L. Search radar detection and track with the Hough transform. II. Detection statistics. *IEEE Transactions on Aerospace and Electronic Systems*, 1994, vol. 30, no. 1, p. 109–115. DOI: 10.1109/7.250411

[21] CARLSON, B. D., EVANS, E. D., WILSON, S. L. Search radar detection and track with the Hough transform. III. Detection performance with binary integration. *IEEE Transactions on Aerospace and Electronic Systems*, 1994, vol. 30, no. 1, p. 116 to 125. DOI: 10.1109/7.250412

[22] CARRETERO-MOYA, J., GISMERO-MENOYO, J., ASENSIO-LOPEZ, A., et al. Application of the Radon transform to detect small-targets in sea clutter. *IET Radar, Sonar & Navigation*, 2009, vol. 3, no. 2, p. 155–166. DOI: 10.1049/iet-rsn:20080123

[23] DENG, X., PI, Y., MORELANDE, M., et al. Track-before-detect procedures for low pulse repetition frequency surveillance radars. *IET Radar, Sonar & Navigation*, 2011, vol. 5, no. 1, p. 65–73. DOI: 10.1049/iet-rsn.2009.0245

[24] GROSSI, E., LOPS, M., VENTURINO, L. A novel dynamic programming algorithm for track-before-detect in radar systems. *IEEE Transactions on Signal Processing*, 2013, vol. 61, no. 10, p. 2608–2619. DOI: 10.1109/TSP.2013.2251338

[25] RAO, X., TAO, H. H., SU, J., et al. Axis rotation MTD algorithm for weak target detection. *Digital Signal Processing*, 2014, vol. 26, p. 81–86. DOI: 10.1016/j.dsp.2013.12.003

[26] KIRKLAND, D. Imaging moving targets using the second-order keystone transform. *IET Radar, Sonar & Navigation*, 2011, vol. 5, no. 8, p. 902–910. DOI: 10.1049/iet-rsn.2010.0304

[27] YANG, J. G., HUANG, X., THOMPSON, J., et al. Low-frequency ultra-wideband synthetic aperture radar ground moving target imaging. *IET Radar, Sonar & Navigation*, 2011, vol. 5, no. 9, p. 994–1001. DOI: 10.1049/iet-rsn.2010.0387

[28] SUN, G., XING, M. D., WANG, Y., et al. Improved ambiguity estimation using a modified fractional Radon transform. *IET Radar, Sonar & Navigation*, 2011, vol. 5, no. 4, p. 489–495. DOI: 10.1049/iet-rsn.2010.0246

[29] YAO, D., ZHANG. X., SUN, Z. Long-time coherent integration for maneuvering target based on second-order keystone transform and Lv's distribution. *Electronics*, 2022, vol. 11, no. 13, p. 1–15. DOI: 10.3390/electronics11131961

[30] WU, L., WEI, X., YANG, D., et al. ISAR imaging of targets with complex motion based on discrete chirp Fourier transform for cubic chirps. *IEEE Transactions on Geoscience and Remote Sensing*, 2012, vol. 50, no. 10, p. 4201–4212. DOI: 10.1109/TGRS.2012.2189220

[31] RAO, X., TAO, H. H., SU, J., et al. Detection of constant radial acceleration weak target via IAR-FRFT. *IEEE Transactions on Aerospace and Electronic Systems*, 2015, vol. 54, no. 4, p. 3242 to 3253. DOI: 10.1109/TAES.2015.140739

[32] RAO, X., TAO, H. H., XIE J., et al. Long-time coherent integration detection of weak manoeuvring target via integration algorithm, improved axis rotation discrete chirp-Fourier transform. *IET Radar, Sonar & Navigation*, 2015, vol. 9, no. 7, p. 917–926. DOI: 10.1049/iet-rsn.2014.0344

[33] SKOLNIK, M. I. *Introduction to Radar System.* 3rd ed. Columbus (OH): McGraw-Hill, 2002. ISBN: 9787121042072

[34] RAO, X., ZHONG, T., TAO, H. H., et al. Improved axis rotation MTD algorithm and its analysis. *Multidimensional Systems and Signal Processing*, 2019, vol. 30, no. 2, p. 885–902. DOI: 10.1007/s11045-018-0588-y

About the Authors …

Xuan RAO was born in Jiangxi Province, P.R. China, in 1977. He received the B.Sc. and M.Sc. degrees from the School of Information Engineering, Nanchang University, Nanchang, China, in 1999 and 2005, respectively; and the Ph.D. degrees from the School of Electronic Engineering, Xidian University, Xi'an, China, in 2015. He is currently an Associate Professor of the School of Information Engineering, Nanchang Hangkong University, China. He is a member of IEEE and his current research interests include radar signal processing, weak target detection and tracking.

Zongying SUN was born in Anhui province, China. He received the B.Eng. degree in Communication Engineering from the Jianghuai College of Anhui University, in 2020. He is currently pursuing the M.S. degree in Signal Processing from the School of Information Engineering, Nanchang Hangkong University. His current research interests include radar signal processing and weak target detection.

Haihong TAO was born in Shanxi Province, China, in 1976. She received the M.Sc. and Ph.D. degrees from the School of Electronic Engineering, Xidian University, Xi'an, China, in 2000 and 2004, respectively. She is currently a Professor of the School of Electronic Engineering, Xidian University. She is also serving as the director of the National Laboratory of Radar Signal Processing at Xidian University. Her research areas are radar signal processing and detection, high-speed real-time signal processing, and array signal processing.